

Graphene quantum dots-gated hollow mesoporous carbon nanoplatform for targeting drug delivery and synergistic chemo-photothermal therapy

Junfeng Fang
Yanqing Liu
Yiwen Chen
Dimei Ouyang
Guangji Yang
Tao Yu

Department of Gynecology, The First People's Hospital of Yunnan Province, Kunming University of Science and Technology, Kunming, P.R. China

Background: Carbon-based drug delivery systems have attracted great interest because of their excellent photothermal conversion capability and high specific surface area for drug loading. Herein, we report a multifunctional nanoplatform based on hyaluronic acid (HA)-modified and graphene quantum dot (GQD)-gated hollow mesoporous carbon nanoparticle (HMCN) for anticancer drug encapsulation and targeted chemo-photothermal therapy of CD44 receptor-overexpressed cancer cells.

Methods: In this design, HMCN was not only used as a nanocarrier with high drug loading content to achieve chemotherapy, but also as a near-infrared absorbing agent to realize photothermal therapy. GQDs could not only prevent premature drug release during blood circulation, but also enhance the chemo-photothermal therapeutic efficacy for complete tumor growth suppression. After being modified with HA, the HA-HMCN(DOX)@GQDs could specifically target cancer cells.

Results: As expected, the as-prepared HMCN exhibited high doxorubicin (DOX)-loading capacity of 410 mg/g and excellent light-to-heat conversion property. The DOX was released from HA-HMCN(DOX)@GQDs in a near-infrared laser and pH stimuli-responsive manner, which could enhance the therapeutic effect. In vitro cell biological experimental results confirmed that the nanoplatform possesses excellent biocompatibility, specifically target CD44 receptor-overexpressing human cervical carcinoma HeLa cells, and has remarkable synergistic chemo-photothermal killing capacity. The in vivo therapeutic studies in HeLa xenografts also showed negligible toxicity of HA-HMCN@GQDs and complete inhibition of tumor growth of HA-HMCN(DOX)@GQDs with near-infrared irradiation.

Conclusion: The excellent therapeutic effects demonstrated in vitro and in vivo suggested the HMCN-based nanoplatform holds potential for efficient dual-responsive targeting drug delivery and synergistic chemo-photothermal therapy.

Keywords: hollow mesoporous carbon nanoparticles, graphene quantum dots, CD44 receptor targeting, chemo-photothermal therapy

Correspondence: Tao Yu
Department of Gynecology, The First People's Hospital of Yunnan Province, Kunming University of Science and Technology, No. 727 South Jingming Road., Chenggong District, Kunming, Yunnan, 650032, P.R. China
Tel +86 871 6363 9921
Fax +86 871 6362 7731
Email yutao1398765971 | @163.com

Introduction

Currently, chemotherapy is one of the most commonly utilized treatments in the clinic with great success in suppressing tumor proliferation and prolonging patient survival.¹⁻³ However, conventional chemotherapy often lacks specificity and selectivity for the cancerous cells, which leads to systemic toxicity. Meanwhile, a single chemotherapy is not powerful in eliminating the whole tumor, especially in preventing cancer metastasis.⁴ To overcome these issues, numerous studies in clinical/exploratory research have focused

on nanotechnology-mediated multimodal synergistic therapy for explaining the significant improvements in therapeutic outcome.⁵⁻⁸ Among them, the combination of chemotherapy and photothermal therapy (PTT) attracted great attention in the past decade.⁹⁻¹² Considering that hyperthermia induced by PTT can enhance tumor accumulation/cell uptake/drug release and result in improving antitumor/antimetastasis efficacy,¹³⁻¹⁵ the naissance of chemo-photothermal synergistic therapy holds great potential to enhance the therapeutic efficacy and reduce the adverse effects. To achieve an ideal therapeutic effect of chemo-photothermal synergistic therapy, the integration of both chemotherapy and photothermal therapeutic functions into a single nanoplatform with the advantages of both in a single therapy offsetting the disadvantages of each monotherapy is still an important issue.

More recently, much effort has been put in to construct synergistic nanoplatforms based on various inorganic or organic materials, such as mesoporous silica,¹⁶ polymers,¹⁷ transition metal dichalcogenides,¹⁸ and sp²-hybridized carbon materials.¹⁹ Among the drug carriers explored, mesoporous carbon nanospheres (MCN) have gained increasing attention due to their high surface area, good biocompatibility, and easily functionalized surface, which can be applied in many fields such as batteries, catalysis, separation, drug delivery, and so on.²⁰⁻²⁴ Also, previous research has shown that MCN exhibited lower toxicity than mesoporous silica nanoparticles (MSNs),²⁵ which makes them more appropriate for biomedical applications. Most importantly, MCN with a high photothermal conversion capability have been successfully used for PTT. Guiju Xu et al reported an efficient nanocarrier based on the functionalized mesoporous carbon nanoparticles for drug delivery and near-infrared (NIR) photothermal conversion for the chemo-photothermal synergistic therapy of HeLa cells.²⁶ Zhou et al²⁷ further explored the photothermal properties of MCN and synthesized the hyaluronic acid (HA)-attached MCN as a multifunctional platform for synergistic chemo-PTT. As a specific member of MCN-based nanofamily, hollow MCN (HMCN) is superior to conventional MCN because the hollow cavity can act as a large reservoir for drug loading and reducing the deposition of foreign materials into bodies subsequently,²⁸ thus significantly enhancing the drug-loading capability of HMCN. To date, only a few HMCN-based nanoplatforms have been explored for drug delivery and PTT. However, still there is a lack of gated HMCN drug delivery systems for stimuli-responsive controlled release.

For the MCN-based drug delivery system, controlled gatekeepers that cap the pore entrances play crucial roles in achieving specific drug release and avoiding premature leakage

during the blood circulation process. To date, various gatekeepers have been designed depending on different requirements, including polymers,^{17,29} inorganic nanomaterials,^{30,31} biomacromolecules,³² and supramolecular assemblies.³³ Among them, graphene quantum dots (GQDs) have attracted growing attention mainly owing to their unique morphology, ease of functionalization, and excellent biocompatibility.³⁴ Qiu et al reported a fluorescent, traceable, and pH-sensitive GQD-based system for doxorubicin (DOX) release and to specifically bind to $\alpha_v\beta_3$ integrins, which are overexpressed in cancer cells.³⁵ Furthermore, the GQDs showed high photothermal conversion efficiency under NIR light irradiation, which can achieve photothermal ablation of xenografted tumor in nude mice.³⁶ More importantly, the excellent photothermal conversion efficiency of GQDs make it not only could serves as an ideal heating gatekeeper to prevent drug from early release during the delivery but also improve the delivery system function with the ability of photothermal therapy and PTT. Yao et al reported promising multifunctional platform based on GQD-capped magnetic MSNs for synergistic therapy with controlled drug release, magnetic hyperthermia, and PTT.³⁷ Also, the oxygen functional groups (hydroxyl, epoxy, and carboxyl groups) on GQDs make it possible to connect them with mesoporous carbon nanoparticles. To the best of our knowledge, there are no previous reports describing the construction of GQD-gated HMCN nanoplatforms for controlled drug delivery and chemo-PTT in potential cancer therapy.

Taking account of the above points, herein, we synthesize a biocompatible HA-modified and GQD-gated HMCN nanoparticle to realize targeted anticancer drug delivery and synergistic chemo-PTT. The hollow cavity in HMCN can act as a large reservoir for improving the drug-loading capacity. The HMCN itself functions as an NIR absorbing agent for inducing mild hyperthermia to achieve tumor photothermal ablation. Then, GQDs were selected as gatekeepers to prevent premature drug release and enhance the chemo-photothermal therapeutic efficacy. In addition, HA was subsequently grafted onto the surface of HMCN through amide bond formation to improve the cancer cell uptake of the nanocarrier, denoted as HA-HMCN(DOX)@GQDs. This versatile nanoplatform could not only achieve a high drug loading content, but could also be recognized and taken up by HeLa cells, and is capable of causing localized mild hyperthermia upon NIR exposure (Figure 1). The structure, morphology, physicochemical properties, drug loading content, drug release manner, and cytocompatibility were well characterized. Then, the synergistic targeted chemo-PTT killing effects of cancer cells in vitro, as well as the therapeutic effects in xenografted tumor model

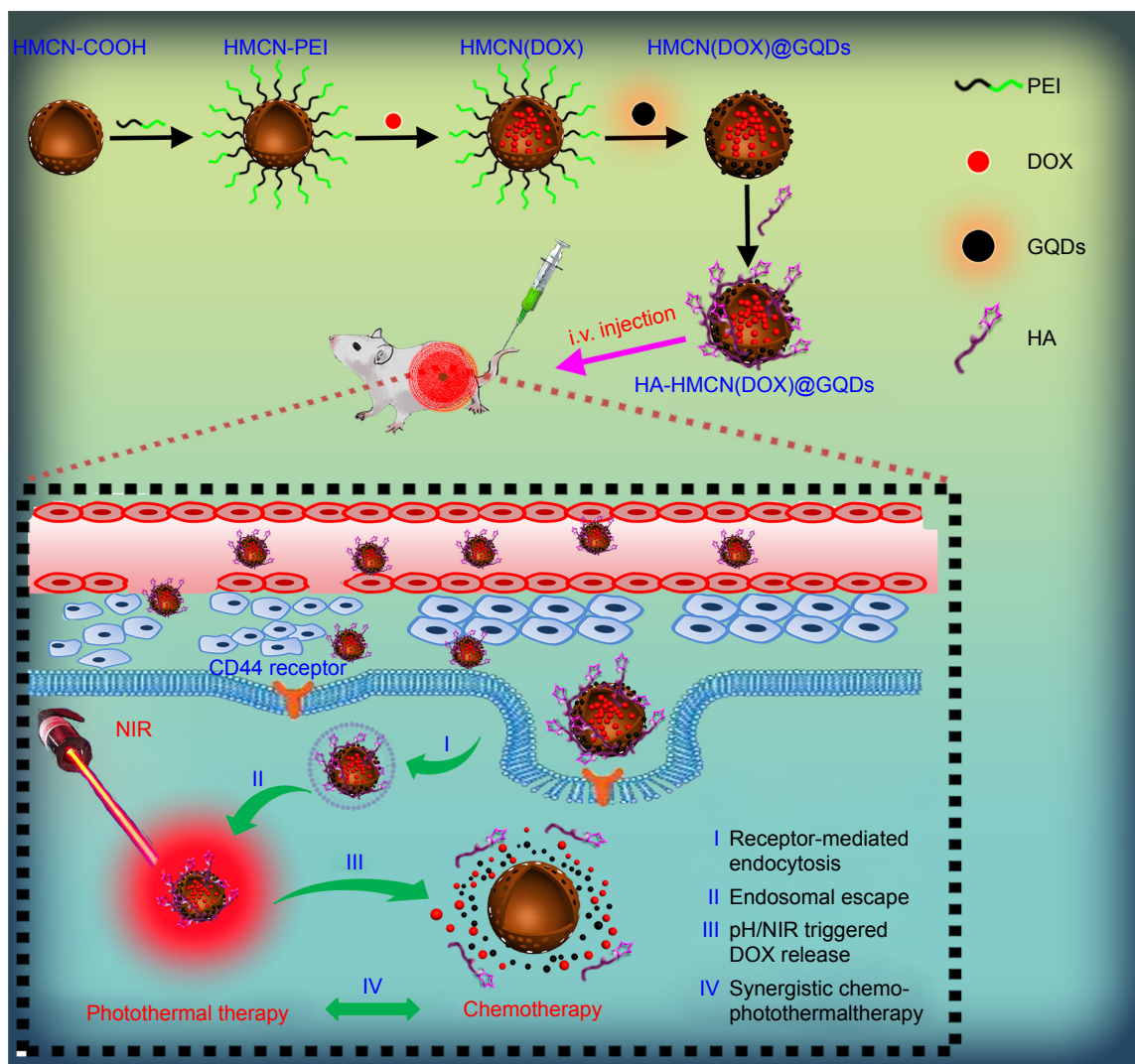


Figure 1 Schematic illustration of HA-HMCN(DOX)@GQDs nanoplatform for targeting drug delivery and synergistic chemo-photothermal therapy.

Abbreviations: DOX, doxorubicin; GQDs, graphene quantum dots; HA, hyaluronic acid; HMCN, hollow mesoporous carbon nanoparticles; NIR, near infrared; PEI, polyethylenimine.

were explored. Our results demonstrated that the combination of these functional elements into single nanoplatform entities significantly enhanced the efficacy of chemotherapy–PTT, which could be a promising nanoplatform for drug delivery and a multimodal therapy for cancer.

Materials and methods

Materials

Cetyltrimethylammonium bromide, tetraethyl orthosilicate (TEOS), oxalic acid, furfural alcohol, ethanol, and ammonia aqueous solution ($\text{NH}_3 \cdot \text{H}_2\text{O}$, 25 wt%) were bought from Sinopharm Chemical Reagent Company (Shanghai, P.R. China). Ammonium persulfate, octadecyltrimethoxysilane (C_{18}TMS), 2-(*N*-morpholino)ethanesulfonic acid (MES), HA, polyethylenimine (PEI; $\text{Mw}=1.8$ kDa), DOX *N*-(3-(dimethylamino)-propyl)-*N*-ethylcarbodiimide (EDC),

and *N*-hydroxysuccinimide (NHS) were purchased from Aladdin Reagent (Shanghai, P.R. China). GQDs (1 mg/mL) were purchased from Nanjing XFNANO Co. Ltd (Nanjing, P.R. China). Calcein-AM, propidium iodide (PI), and MTT were purchased from Sigma-Aldrich (St Louis, MO, USA). Roswell Park Memorial Institute (RPMI)-1640 medium, FBS, and penicillin–streptomycin were supplied by Thermo Fisher Scientific (Waltham, MA, USA). The HeLa cells (a human cervical carcinoma cell line) were bought from Cyagen Biosciences Inc. (Guangzhou, P.R. China).

Preparation of HMC-COOH nanoparticles

The sSiO_2 spheres were prepared following the Stöber method with slight modification.³⁸ Six milliliters of TEOS was added to a mixture of 142.8 mL ethanol, 20 mL H_2O , and 3.14 mL

ammonia solution, which was stirred for 2 hours at 35°C. The sSiO₂ nanospheres were harvested by centrifugation, purified by ethanol and water for several times, and dried under vacuum. Then, the as-prepared sSiO₂ spheres were dispersed in a mixture containing 80 mL ethanol and 2.5 mL ammonia solution, which was vigorously stirred at 35°C for 1 hour. Five milliliters of TEOS and 2 mL of C₁₈TMS were then mixed and added to the above mixture, which was magnetically stirred for another 1.5 hours. Thereafter, the final products were collected by centrifugation, washed with deionized water for several times, followed by calcining at 550°C for 6 hours to form sSiO₂@mesoporous SiO₂ templates.

HMCN nanoparticles were prepared following a previous study.^{9,39} The carbon precursor was prepared by dissolving 10 mg of oxalic acid in 1 mL of furfuryl alcohol. Then, the carbon precursor was filled into the pores of the as-prepared sSiO₂@mSiO₂ templates. The solution was stirred at 60°C for 15 hours, and the temperature was increased to 80°C for another 15 hours in a Teflon-lined autoclave and then carbonized for 3 hours at 700°C under a nitrogen atmosphere. Thereafter, the above mixture was dispersed in 10% hydrofluoric acid for 24 hours and then washed several times with distilled water. The black products were dried in vacuum and denoted as HMCN. For the carboxylation of HMCN, 0.5 g of HMCN nanoparticles was dispersed in a solution containing 30 mL of 0.25 M ammonium persulfate solution and 1.6 mL H₂SO₄. The mixture was stirred with reflux at 60°C for 3 hours, and the carboxylated HMCN was harvested by centrifugation and repeatedly purified by ethanol and water up to neutral pH and dried under a vacuum to obtain HMSN-COOH.

Preparation of HMCN-PEI

Briefly, 20 mg of HMSN-COOH in MES buffer (50 mM, pH 6) was mixed with 20 mg of EDC and 16 mg of NHS. This mixture was reacted for 2 hours at ambient temperature to activate the carboxyl. Subsequently, excess PEI was added and stirred for 24 hours. The obtained HMCN-PEI was dialyzed (molecular weight cut-off: 3,500 Da; 4,000 rpm) against MES buffer for three times and washed with pure water to remove the unreacted PEI.

DOX loading, GQDs capping, and HA grafting

Drug loading was carried out by dispersing HMCN-PEI (20 mg) in a 10 mL PBS solution (pH 7.4) containing 10 mg DOX and stirring for 24 hours at room temperature in the dark. The DOX-loaded HMCN-PEI nanoparticles (HMCN(DOX)) were centrifuged and washed with PBS to

remove the unbound DOX. Meanwhile, the drug loading content was calculated by ultraviolet (UV)–visible (Vis) spectrophotometry at 480 nm following the equation:

$$LC = \frac{\text{Initial mass of the DOX} - \text{The mass of DOX in the supernatant}}{\text{Mass of DOX loaded nanocarriers}} \times 100\% \quad (1)$$

The outlets of HMCN(DOX) nanoparticles were capped with GQDs through covalent amide linkage between the amine group in PEI and the carboxyl of GQDs. Briefly, GQDs (20 mL, 1 mg/mL) were activated by EDC (35 mg) and NHS (20 mg), which were dissolved in H₂O. Then, 20 mg of HMCN(DOX) nanoparticles was slowly added into the activated GQDs solution. After stirring for 24 hours in dark at 4°C, the GQDs-gated HMCN(DOX) nanoparticles (HMCN(DOX)@GQDs) were collected by centrifugation and copiously washed with the buffer solution to rinse the residual EDC, NHS, and GQDs. Then, the HMCN(DOX)@GQDs was redispersed in 10 mL of water for further use. Next, 25 mg HA was dissolved in pH 7.4 PBS, and an aqueous solution of EDC (28.7 mg, 1 mL) was added and stirred vigorously at room temperature for 0.5 hour. Next, NHS (16.4 mg, 1 mL) was added under stirring for 2.5 hours. Subsequently, the above HMCN(DOX)@GQDs solution was added to the HA solution, followed by allowing it to react for another 24 hours. The final HA-modified HMCN(DOX)@GQDs nanoparticles, which were denoted as HA-HMCN(DOX)@GQDs, were obtained by centrifugation. Meanwhile, the HA-HMCN@GQDs nanoparticles were prepared by using the same process, but without DOX loading.

Characterization

The morphology and structure of the as-prepared nanoparticles were examined by transmission electron microscopy (TEM; JEM-2100; JEOL, Tokyo, Japan). Nitrogen adsorption/desorption isotherms and pore size distributions were obtained with an adsorption analyzer (Micromeritics, Norcross, GA, USA). Fourier-transform infrared spectra were measured on a Nexus 670 spectrometer (Thermo Fisher Scientific). The wide-angle X-ray diffraction (XRD) patterns were obtained on a D8 ADVANCE powder diffractometer using Cu K_{α1} radiation (1.5405 Å). Dynamic light scattering was conducted by using a BI-200SM multiangle dynamic/static laser scattering instrument (Brookhaven Instruments Corporation, Holtsville, NY, USA). Zeta potential was detected by a Zetasizer Nano ZS Nanosizer (Malvern Instruments, Malvern, UK). UV-Vis spectra were recorded on a UV-3101PC Shimadzu spectroscope (Shimadzu, Kyoto, Japan). The content

of Si was determined by Agilent 5110 inductively coupled plasma-optical emission spectroscopy (Agilent Technologies, Santa Clara, CA, USA).

Photothermal performance measurement of HA-HMCN@GQDs

To measure the photothermal conversion effect of HA-HMCN@GQDs nanocomposites, different concentrations of HA-HMCN@GQDs dispersion solution (5, 10, 25, 50, and 100 $\mu\text{g/mL}$) in a 1.5 mL Eppendorf tube were exposed to an 808 nm laser (SFOLT Co., Ltd, Shanghai, P.R. China) at 1.0 W/cm^2 for 5 minutes. The spot-effective area of the laser light source was about 0.25 cm^2 . A thermocouple thermometer (DT-8891E; Shenzhen Everbest Machinery Industry Co., Ltd, Shenzhen, P.R. China) was employed to measure the temperature profiles during irradiation. Then, the HA-HMCN@GQDs dispersion solution at the same concentration (100 $\mu\text{g/mL}$) was irradiated with different power densities (ie, 0.25, 0.5, 1.0, and 1.5 W/cm^2) over a period of 5 minutes. For these power densities, the corresponding total energy doses were 75, 150, 300, and 450 J/cm^2 , respectively. Meanwhile, the temperature profiles of the pure water, HMCN, and GQDs solutions were also measured. Furthermore, the photostability of HA-HMCN@GQDs was detected using on-off cycles of NIR laser irradiation.

In vitro dual-stimuli responsive drug release

To evaluate the pH and NIR dual-stimuli responsive DOX release, 20 mg of the HA-HMCN(DOX)@GQDs nanoparticles was dispersed in 10 mL of PBS solution at pH 5.0 or 7.4 with or without NIR laser irradiation. The solution was shaken at 130 rpm (37°C) in dark. For NIR-triggered groups, the sample solutions were exposed to 808 nm NIR laser radiation (1.0 W/cm^2) for 5 minutes. After a predetermined time interval, 1 mL sample of the release solutions was taken from the suspension and an equal volume of fresh medium was supplemented. The released amount of DOX was measured by using UV-Vis spectroscopy at 480 nm.

In vitro cellular uptake of HA-HMCN(DOX)@GQDs

The HeLa cells were cultured in RPMI-1640 cell culture medium supplemented with 10% FBS and 1% penicillin/streptomycin at 37°C in 5% CO_2 . After incubation for 24 hours, the medium was removed and replaced with 200 μL of RPMI-1640 medium containing 5 $\mu\text{g/mL}$ DOX equivalent of HA-HMCN(DOX)@GQDs, HMCN(DOX)@GQDs, or

free DOX. The cells were carefully washed three times with cold PBS following 4 hours of incubation. Thereafter, the cells of the photothermal group were irradiated with a laser (808 nm, 1 W/cm^2 , 5 minutes) after 2 hours of incubation and were cultured for an additional 2 hours. The cells in all the groups were washed and fixed with 4% formaldehyde for 30 minutes. Subsequently, DAPI was used to stain the nuclei and the DOX distribution was observed by confocal laser scanning microscopy (CLSM; Carl Zeiss Meditec AG, Jena, Germany).

In vitro cytotoxicity and chemo-PTT

The cytotoxicity and the synergistic chemo-PTT efficacy of the HA-HMCN(DOX)@GQDs against HeLa cells were evaluated by MTT assay. In brief, HeLa cells were seeded in 96-well plates at a density of 2.0×10^4 cells/well and incubated for 24 hours. Then, the cells were incubated with blank carriers (HA-HMCN@GQDs), different nanoparticles, and free DOX with different concentrations of DOX (0.01, 0.1, 1.0, 5.0, and 10.0 $\mu\text{g/mL}$) for 4 hours. For the NIR irradiation groups, the cells were irradiated by an 808 nm laser at an output power of 1 W/cm^2 for 5 minutes. After incubation for another 2 hours, the cells were washed with PBS and incubated in fresh medium for 24 hours. Afterward, 100 μL of MTT solution (0.5 mg/mL) was added and incubated for another 4 hours. Then, 100 μL of dimethyl sulfoxide was added to dissolve the intracellular formazan crystals and the absorbance of the solution was measured at 570 nm by a microplate reader (BioTek, Winooski, VT, USA). Meanwhile, the untreated cells in the growth media were used as the blank control.

The cell live/dead assays were carried out to further evaluate the therapeutic efficiency of different treatments. Briefly, HeLa cells were seeded into a 24-well plate at a density of 5×10^3 per well. After being incubated for 24 hours, the cells of different groups were treated with PBS, free DOX, HA-HMCN@GQDs with laser irradiation (1.0 W/cm^2 , 5 minutes), HA-HMCN(DOX)@GQDs only, and HA-HMCN(DOX)@GQDs with laser irradiation (1.0 W/cm^2 , 5 minutes), respectively. After washing several times with PBS, the cells were stained with both calcein AM and PI for 40 minutes. Finally, the cells were washed and imaged using an Olympus IX71 microscope (Olympus, Glasgow, UK).

Cell apoptosis analysis

HeLa cells were seeded in six-well plates at a density of 5×10^4 cells per well and incubated for 24 hours. Subsequently, the cells were treated with different formulations at a DOX concentration

of 10 $\mu\text{g}/\text{mL}$. Then, the cells were incubated with fresh medium without NIR laser irradiation or with NIR light irradiation (1.0 W/cm^2 , 5 minutes). The cells without any treatment were used as a control. Then, all of the cells were collected and resuspended in 0.5 mL PBS. After that, all cells were stained with PI and Annexin V-fluorescein isothiocyanate (FITC) containing binding buffer for 15 minutes and finally detected by flow cytometry (Becton Dickinson, San Jose, CA, USA).

Xenograft tumor models and in vivo antitumor efficacy

Female nude mice (20–25 g) were provided by the Animal Center of Kunming Medical University (Kunming, P.R. China) and were used for the animal experiments directly. All animal experimental procedures were performed following protocols approved by the Institutional Animal Care and Use Committee of the Animal Center of Kunming Medical University (Kunming, P.R. China) and all the animals were treated in accordance with the First People's Hospital of Yunnan Province's guidelines. Ethical approval for all experiments was obtained from the Animal Center of Kunming Medical University (Kunming, P.R. China) before beginning the in vivo work. The tumor models were obtained by injecting female mice with HeLa cells (5×10^7 cells) subcutaneously on the right front flank. The length (L) and width (W) of the tumor were measured with a caliper. The tumor size was calculated with the following formula:

$$V = 1/2 \times L \times W^2 \quad (2)$$

In vivo experiments were carried out when the tumor size reached to about 100 mm^3 . Tumor-bearing mice were randomly divided into six groups ($n=4$). The mice were treated with 1) PBS; 2) free DOX (dose=5 mg/kg DOX); 3) HMCN(DOX)@GQDs (dose=5 mg/kg DOX); 4) HA-HMCN(DOX)@GQDs (5 mg/kg DOX); 5) HA-HMCN@GQDs plus NIR laser (5 mg/kg DOX); or 6) HA-HMCN(DOX)@GQDs plus NIR laser (5 mg/kg DOX). All mice were injected via the tail vein on day 1, 3, and 5. Mice in groups 5 and 6 were irradiated by the laser at 1 W/cm^2 for 10 minutes at 8 hours postinjection. The weight of the mice and the tumor volume were measured every 3 days.

For in vivo fluorescence imaging, mice with HeLa tumors were intravenously (i.v.) injected with HA-HMCN(DOX)@GQDs (dose=5 mg/kg DOX). Then, the mice were irradiated by the laser at 1 W/cm^2 for 10 minutes at 2 hours postinjection. Afterward, in vivo fluorescence imaging at different time points (2, 4, 12, 24, and 48 hours) was carried out using a Lumina III in vivo imaging system (PerkinElmer Inc., Waltham, MA, USA) to check the DOX fluorescence.

Histological staining

Mice were sacrificed at 18 days after different treatments and the tumors were excised and weighed. Simultaneously, the main organs including liver, heart, kidney, spleen, and lung of the mice were also collected and fixed using 4% paraformaldehyde. H&E staining was performed to evaluate the biocompatibility. Moreover, the tumor tissues in each group were fixed in 10% formalin, sectioned, and stained with H&E and standard TUNEL. Finally, the morphology of the tumor/tissues sections of each group was observed using an optical microscope (Leica, Barnack, Germany) to evaluate the antitumor mechanism.

In vivo pharmacokinetic assay

To evaluate the blood circulation profile of the HA-HMCN(DOX)@GQDs nanoparticles, the HeLa tumor-bearing mice ($n=4$) were i.v. injected with 200 μL of DOX and HA-HMCN(DOX)@GQDs at the same DOX dose of 5 mg/kg. Thereafter, $\sim 20 \mu\text{L}$ of blood was withdrawn from each mouse at predestined time intervals (0.5, 2, 4, 8, 12, and 24 hours). Each blood sample was dissolved in 1 mL of lysis buffer, and 300 μL of hydrochloric acid-isopropanol (HCl-IPA) was added to extract DOX from blood. After centrifugation, the amount of DOX in all samples was measured by fluorescence measurement and the pharmacokinetics analysis was performed with Win NonLin 6.3 software (Pharsight, Mountain View, CA, USA).

Statistical analysis

Data were presented as mean \pm SD. Student's *t*-test was applied to test the significance of the difference. $P < 0.05$, $**P < 0.01$, and $***P < 0.001$ were considered as statistically significant.

Results and discussion

Preparation and characterization of HA-HMCN(DOX)@GQDs nanoparticles

Figure 1 shows the schematic illustration of fabrication of the HA-HMCN(DOX)@GQDs nanopatform for controlled drug release, targeted drug delivery, and synergistic chemo-PTT. HMCN was prepared by using sSiO_2 @ mSiO_2 sphere as the template via the modified Stober method as described in the literature.^{9,39} Furfuryl alcohol was chosen as the carbon precursor and filled in the templates. Then, the mixture was polymerized and calcinated under nitrogen to form the C-Si structure. Afterward, the C-Si mixture was also treated in HF solution to etch away the Si part and HNCN was prepared. The morphology of HMCN was characterized by TEM (Figure 2A), where HMCN with uniform hollow cavity and well-defined

mesoporous shell was observed, resulting in high drug loading capacity (inset of Figure 2A). Also, the average diameter of the nanoparticles was about 120 nm. The TEM image showed that GQDs with a diameter of around 5 nm were capped on the surface of HMCN(DOX) nanoparticles (Figure 2B). From N_2 adsorption–desorption analysis, the Brunauer–Emmett–Teller (BET) specific surface area and pore size of HMCN was calculated to be 886.37 m^2/g and 3.12 nm, respectively (Figure 2C and D). These results demonstrated that the obtained HMCN was suitable for drug delivery.

To improve the dispersibility and hydrophilicity of HMCN, the carboxyl groups were introduced to the outer surfaces of HMCN. The zeta potential of HMCN was about -13.4 mV, which changed to -34.3 mV after carboxylation (Figure 3A). Also, the stretching vibration of

carbonyl groups around $1,705$ and $3,436$ cm^{-1} was observed in the Fourier-transform infrared spectrum of HMCN-COOH (Figure 3B), which confirmed the success of carboxylation functionalization. Then, PEI was covalently conjugated to HMCN-COOH via amide bond reaction to form HMCN-PEI. After PEI conjugation, two strong bands at $1,637$ and $1,487$ cm^{-1} were observed corresponding to amide I and amide II groups, respectively. Meanwhile, a positive value of $+31.4$ mV was obtained for HMCN-PEI (Figure 3A). From a viewpoint of particle size and mesoporous structure, the HMCN nanoparticles could be used as nanocarriers for drug delivery. After DOX loading, the absorption peaks of DOX at 480 nm appeared, demonstrating that DOX was loaded into the HMCNs successfully (Figure 3C). Meanwhile, the drug loading content of HMCN-PEI was calculated to be 410 mg/g

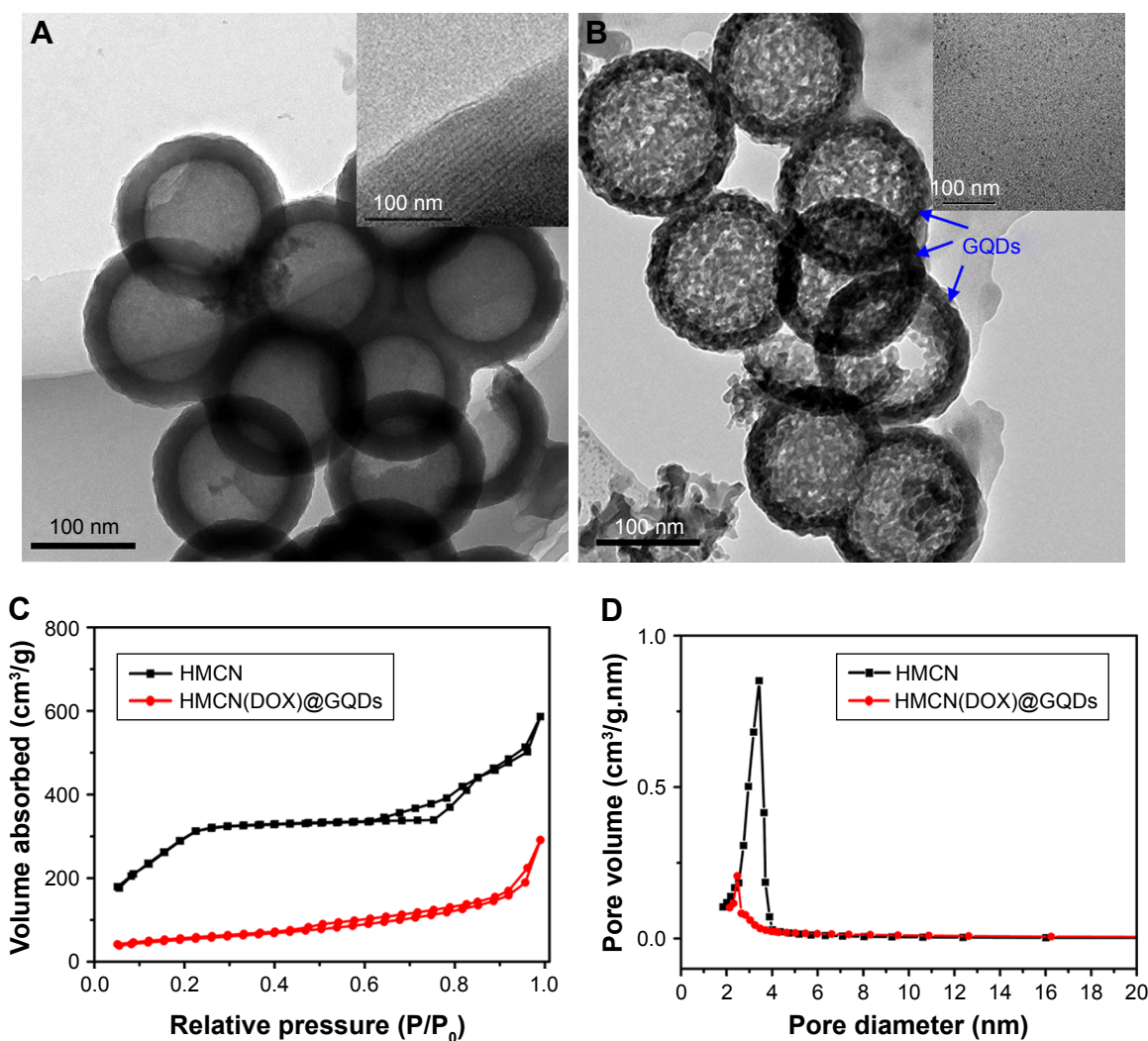


Figure 2 Characterizations of the nanoparticles.

Notes: (A) TEM images of HMCN and the mesoporous shell of HMCN (inset). (B) TEM images of HA-HMCN(DOX)@GQDs and GQDs (inset). (C) N_2 adsorption–desorption isotherm and (D) the corresponding pore size distribution curve of HMCN and HMCN(DOX)@GQDs.

Abbreviations: DOX, doxorubicin; GQDs, graphene quantum dots; HA, hyaluronic acid; HMCN, hollow mesoporous carbon nanoparticles; TEM, transmission electron microscopy.

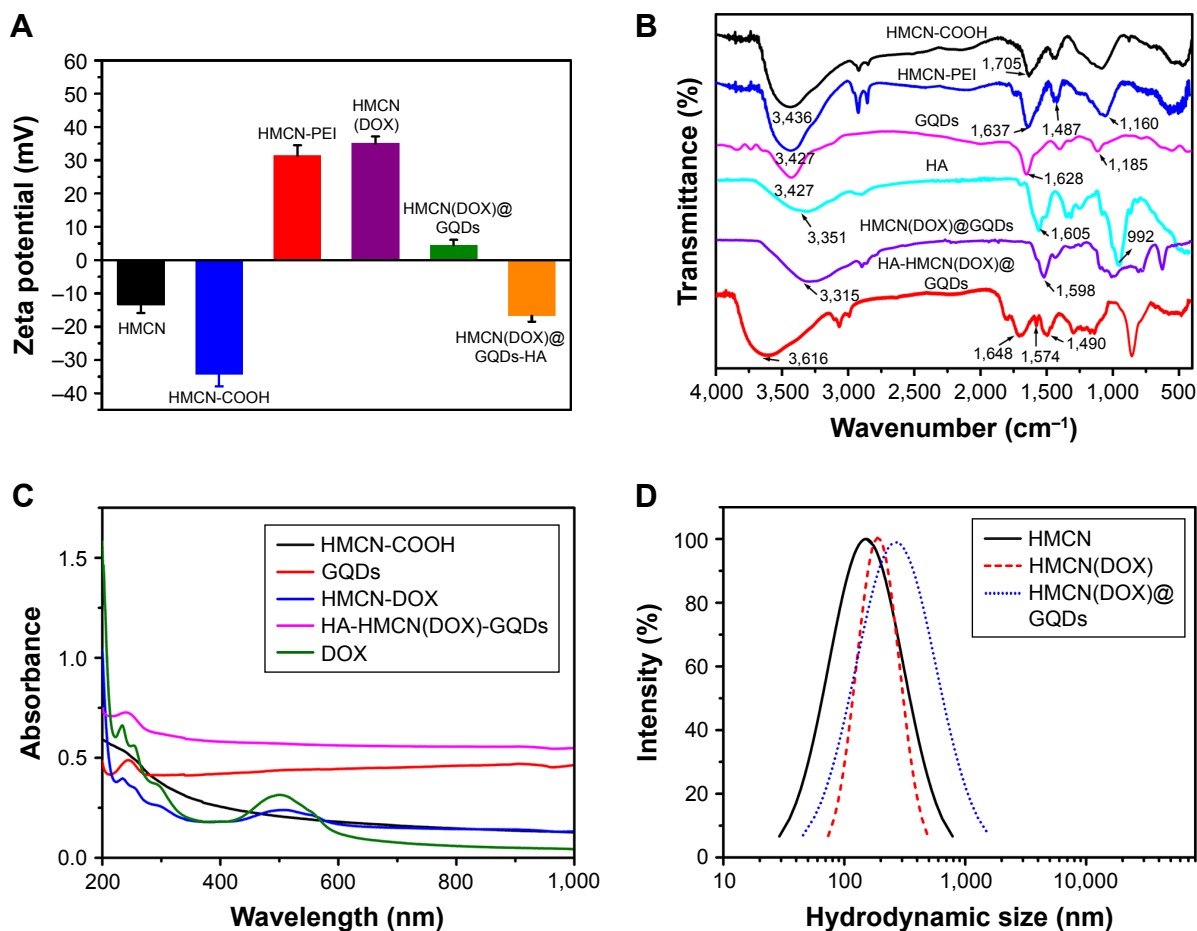


Figure 3 Physicochemical properties of HA-HMCN(DOX)@GQDs nanoparticles.

Notes: (A) The surface charge potentials of different nanoparticles. (B) FT-IR spectra of HMCN-COOH, HMCN-PEI, GQDs, HA, HMCN(DOX)@GQDs, and HA-HMCN(DOX)@GQDs. (C) UV-Vis spectrum of different nanoparticles' aqueous dispersion. (D) Size distribution of HMCN, HMCN(DOX), and HMCN(DOX)@GQDs.

Abbreviations: DOX, doxorubicin; FT-IR, Fourier-transform infrared spectroscopy; GQDs, graphene quantum dots; HA, hyaluronic acid; HMCN, hollow mesoporous carbon nanoparticle; PEI, polyethylenimine; UV-Vis, ultraviolet-visible.

HMCN-PEI and a high drug entrapment efficiency of 96.7% was achieved, which is much higher than that of other drug carriers, indicating the high drug loading capacity of HMCN. Next, GQD was used as a capping agent to seal the pore through the interaction between the carboxyl groups on GQDs and the amino groups on PEI. Thus, the HMCN(DOX)@GQDs nanoparticles were formed. The dynamic light scattering results (Figure 3D) also indicated the hydrodynamic diameter of HMCN(DOX)@GQDs was 206 nm, which is slightly higher compared to those of HMCN-COOH nanoparticles (148 nm) and HMCN(DOX) (162 nm). Meanwhile, the GQD gating was also confirmed by XRD. As shown in Figure S1, no diffraction peaks were observed for HMCN(DOX), while a broad diffraction peak corresponding to GQDs at $2\theta=9^\circ$ was observed for HMCN(DOX)@GQDs, which also indicated GQDs capping on the HMCN(DOX) nanoparticles.³⁵ Moreover, the surface area decreased to 145 m²/g after DOX and GQDs capping, and no obvious pore size distribution in the mesopore range was observed (Figure 2D). This may be

attributed to the closure of the pores by the capping effect of GQDs attached to HMCN. Finally, the HA was coated onto hybrid HMCN(DOX)@GQDs to obtain the versatile nanoplatform (HA-HMCN(DOX)@GQDs). The zeta potential reversed from 4.5 mV of HMCN(DOX)@GQDs to -16.7 mV of HA-HMCN(DOX)@GQDs because of the highly negative charge of the carboxyl groups, which indicated that the HA nanoparticles were successfully modified. In addition, the HA-HMCN(DOX)@GQDs nanoparticles showed good dispersity in water, PBS, and RPMI, suggesting that the developed HA-HMCN(DOX)@GQDs nanoparticles possessed good colloidal stability (Figure S2). On the other hand, the spectra of the HA-HMCN(DOX)@GQDs nanoparticles exhibited a new stretching vibration of -CONH- at 1,574 and 1,648 cm⁻¹, which indicates the interaction between the carboxyl groups of GQDs and the amino groups of PEI. Taken together, these data suggest that the HMCN nanocarrier could load DOX, be capped by GQDs, and conjugate HA to form a multifunctional platform with the potential combination

of targeted drug delivery, dual-responsive drug release, and chemotherapy-PTT.

In vitro photothermal effect of HA-HMCN(DOX)@GQDs

Encouraged by the excellent photothermal properties of HMCN and the ability of GQDs caps to also convert NIR light energy into thermal energy, the photothermal synergistic effect of HA-HMCN(DOX)@GQDs was evaluated. The temperature change of HA-HMCN(DOX)@GQDs suspensions with different concentrations (5, 10, 25, 50, and 100 $\mu\text{g/mL}$) that were exposed to 808 nm NIR irradiation (1.0 W/cm^2) for 5 minutes was monitored (water was selected as the control). As shown in Figure 4A, the temperature of the HA-HMCN(DOX)@GQDs samples increased rapidly under continuous NIR irradiation, while only slight increase was detected in water. Meanwhile,

the concentration-dependent temperature increases for HA-HMCN(DOX)@GQDs suspensions were observed. Similarly, the photothermal performance was dependent on the irradiation power density (Figure 4B). In addition, at the same concentration and power, the temperature of HA-HMCN(DOX)@GQDs solution was higher than HA-HMCN(DOX), demonstrating the synergistic light-to-heat effect of HMCN and GQDs in the enhancement of photothermal efficiency due to GQDs conjugation (Figure 4C). Then, the photothermal stability of HA-HMCN(DOX)@GQDs was studied by five cycles of laser irradiation. As observed in Figure 4D, almost no noticeable attenuation was observed after five cycles of laser irradiation. On the other hand, the UV-vis spectrum curves of HA-HMCN(DOX)@GQDs suspension had negligible changes after irradiation (Figure 4E). These results demonstrated that the obtained HA-HMCN(DOX)@GQDs nanoparticles

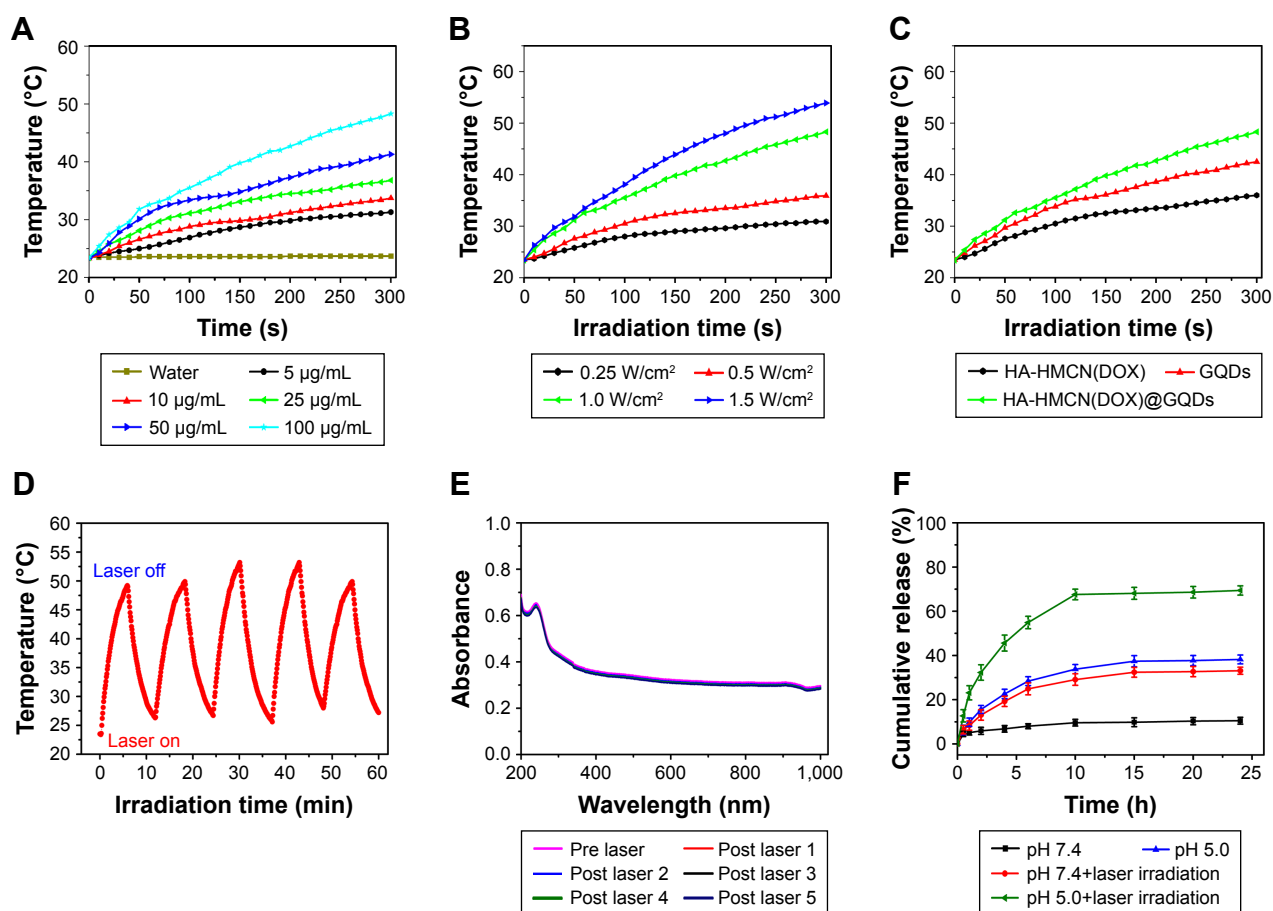


Figure 4 In vitro photothermal effect and stability of HA-HMCN(DOX)@GQDs and drug release behavior.

Notes: Temperature increase profiles of HA-HMCN(DOX)@GQDs dispersion solution (**A**) at different concentrations upon NIR laser irradiation (power density: 0.5 W/cm^2) for 5 minutes and (**B**) at different power densities (concentration of HA-HMCN(DOX)@GQDs: $100 \mu\text{g/mL}$) for 5 minutes. (**C**) Temperature increase profiles of HA-HMCN(DOX), GQDs, and HA-HMCN(DOX)@GQDs dispersion solutions at uniform concentration and power. (**D**) Photothermal stability of HA-HMCN(DOX)@GQDs within five cycles of NIR laser irradiation. (**E**) Absorption spectra of the HA-HMCN(DOX)@GQDs after NIR irradiation for five cycles. (**F**) Cumulative DOX release from the HA-HMCN(DOX)@GQDs nanoparticles under different pH values with and without 808 nm laser irradiation.

Abbreviations: DOX, doxorubicin; GQDs, graphene quantum dots; HA, hyaluronic acid; HMCN, hollow mesoporous carbon nanoparticle; NIR, near infrared.

would be a promising photothermal agent for PTT, and that the combination of HMCN and GQDs would be a more ideal photothermal agent than the MSN-based chemophotothermal nanoplatfoms.^{10,13,15}

In vitro DOX release behavior

To evaluate the drug release behavior, the HA-HMCN(DOX)@GQDs nanoparticles were dispersed in the release medium (pH 7.4 or 5.0) with and without NIR laser irradiation (808 nm, 1.0 W/cm², 5 minutes), respectively. Without NIR laser stimulation, <11% of the DOX was released from the HA-HMCN(DOX)@GQDs in the neutral condition (pH 7.4), while the released DOX was increased to 38% in pH 5.0 PBS (Figure 4F). This was mainly because the weakly acidic condition reduced the interaction between GQDs and HMCN and also decreased the electrostatic interaction between DOX and HMCN.³¹ Meanwhile, the amount of DOX released was obviously increased with laser irradiation, which increased to 69.42% under NIR irradiation at pH 5.0. The light-triggered DOX release enhancement is mainly attributed to the dissociation of the interactions (π - π stacking and pore adsorption) between DOX and HMCN caused by the heat generated by HMCN and GQDs upon laser irradiation.⁴⁰ Furthermore, the in vitro drug release from HA-HMCN(DOX) was studied to verify the gating effect of GQDs. As presented in Figure S3, an obvious burst release was observed with >70% DOX release from HA-HMCN(DOX) at pH 7.4, while the DOX release from the HA-HMCN(DOX)@GQDs at pH 7.4 was <11% over 24 hours, indicating an excellent gating effect of GQDs. Taken together, these results demonstrated that the NIR light irradiation can not only induce mild hyperthermia for PTT, but also achieve NIR-responsive drug release for the synergistic therapy of chemotherapy and PTT.

Considering the fact that the tumor microenvironment is mildly acidic with a pH range of 5.8–7.1 and the intracellular environment is even more acidic, DOX was released from the nanoplatfom once HA-HMCN(DOX)@GQDs entered the cells. Further drug release was triggered by the hyperthermia that was generated by HMCN and GQDs upon laser irradiation. So, the pH/laser dual-stimuli-responsive HA-HMCN(DOX)@GQDs are expected to be applied to “on demand” chemotherapy of cancer, and HA-HMCN(DOX)@GQDs can also serve as a photothermal agent to induce hyperthermia for PTT.

In vitro targeted cellular uptake

Targeted uptake of nanocarriers is particularly beneficial for facilitation of specific tumor accumulation and cancer

cells’ internalization. Thanks to the decoration of HA, the HA-HMCN(DOX)@GQDs could have increased targeting capability for CD44-overexpressed cancer cells. Due to the CD44 receptors overexpressed on the membrane, HeLa cells were employed to investigate the targeting ability of nanoparticles by CLSM.⁴¹ The nuclei of the HeLa cells were stained blue by DAPI and the red fluorescence of DOX in the cells was monitored (Figure 5A). For each group, the DOX concentration (5 μ g/mL) was kept constant. It can be observed that the free DOX was mainly localized in the nucleus due to the high affinity between DOX and DNA.⁴² Owing to the HA modification, the red fluorescence of HA-HMCN(DOX)@GQDs was significantly higher than that of HMCN(DOX)@GQDs, indicating HA-HMCN(DOX)@GQDs nanoparticles can efficiently target HeLa cells and also efficiently deliver and release DOX into the nuclei of the cells. Besides, the DOX signal in HA-HMCN(DOX)@GQDs was further enhanced after treatment with laser irradiation (1 W/cm², 5 minutes), which corroborated the enhanced cellular uptake of HA-HMCN(DOX)@GQDs under laser irradiation. This phenomenon may be attributed to the local mild hyperthermia that could enhance the cell permeability and fluidity, thus further improving the intracellular uptake of nanoparticles.⁴³ To further validate these results, the amount of Si element in HeLa cells after different treatments was determined by inductively coupled plasma-optical emission spectroscopy. As shown in Figure 5B, cells treated with HA-HMCN(DOX)@GQDs showed higher level of Si than those treated with HMCN(DOX)@GQDs. Also, the uptake of Si in laser irradiation group was as high as nearly 1.6-fold of that in HA-HMCN(DOX)@GQDs without laser irradiation, which is consistent with the CLSM results. These results suggested the incorporation of HA could improve the uptake of HA-HMCN(DOX)@GQDs into HeLa cells and the laser irradiation also could further improve the cell uptake.

In vitro cell viability analysis

To evaluate the biocompatibility of the obtained nanocarrier, the cell viability of HA-HMCN@GQDs at a series of DOX concentrations toward HeLa cells was evaluated by MTT assay. It can be observed that HA-HMCN@GQDs caused negligible toxicity to HeLa cells and the cell viability was found to be over 80% even at high concentrations (200 μ g/mL), suggesting the excellent biocompatibility of HA-HMCN@GQDs (Figure S4). The cytotoxic effects of different treatments, including single chemotherapy, PTT, and synergistic chemo-PTT, were studied upon drug loading. The results showed that the viability of cells treated

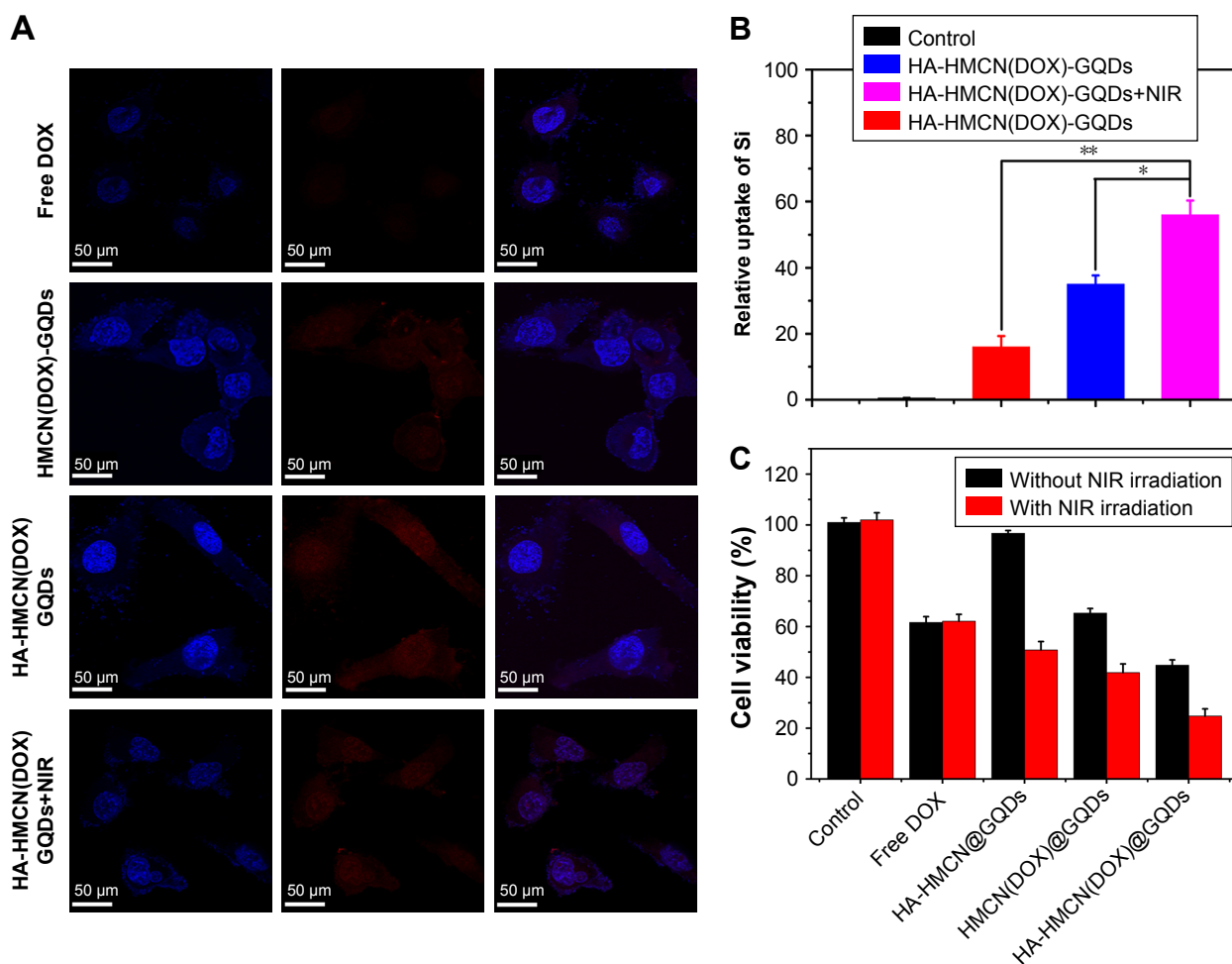


Figure 5 In vitro targeted cellular uptake and cell viability.

Notes: (A) CLSM images of HeLa cells treated with different formulations after 4 hours of incubation (DOX concentration: 5 $\mu\text{g}/\text{mL}$). Scale bar: 50 μm . (B) The mass of silicon internalized in HeLa cells after treatment with different formulations. $*P < 0.05$ and $**P < 0.01$. (C) Cell viability of the HeLa cells after 8 hours of incubation with different formulation suspensions (DOX: 5 $\mu\text{g}/\text{mL}$) with and without NIR irradiation for 5 minutes.

Abbreviations: CLSM, confocal laser scanning microscopy; DOX, doxorubicin; GQDs, graphene quantum dots; HA, hyaluronic acid; HMCN, hollow mesoporous carbon nanoparticle; NIR, near infrared.

with different drug formulations significantly decreased, and also, a drug concentration-dependent cell inhibition was observed (Figure S4). As shown in Figure 5C, the viability of cells treated with HA-HMCN(DOX)@GQDs was lower than that of cells treated with HMCN(DOX)@GQDs, which is especially attributed to the fact that the uptake of HA-HMCN(DOX)@GQDs mediated by the CD44 receptors could increase the antitumor activity of chemotherapy. Meanwhile, nearly 50% of cells were killed in HA-HMCN@GQDs with NIR irradiation group, which confirmed the excellent photothermal therapeutic efficiency. As expected, the HeLa cells treated with the HA-HMCN(DOX)@GQDs nanoparticles and NIR irradiation exhibited an excellent synergistic therapeutic effect of chemotherapy and PTT as compared to those of chemotherapy and PTT alone, and the cell viability further decreased to 24.8%. To further assess the chemo-photothermal effect, HeLa cells were co-stained with calcein AM (live

cells, green) and PI (dead cells, red) after different treatments (Figure 6A). It could be observed that most of the cells were suppressed in the synergistic group (HA-HMCN(DOX)@GQDs plus laser). In contrast, other groups showed less dead cells to some content, corroborating with the results obtained in MTT test. Overall, these results demonstrated that HA-HMCN(DOX)@GQDs may have enormous potential to achieve chemo-photothermal ablation effect of cancer.

In vitro cell apoptosis assay

Flow cytometry analysis was used to further evaluate chemo-photothermal effect. The HeLa cells were treated with various formulations, and Annexin V-FITC and PI double staining was conducted to analyze these cells by flow cytometry. As shown in Figure 6B and C, without NIR irradiation, the cells treated with free DOX and HA-HMCN(DOX)@GQDs displayed slightly increased cell apoptosis (the rate of apoptotic cells

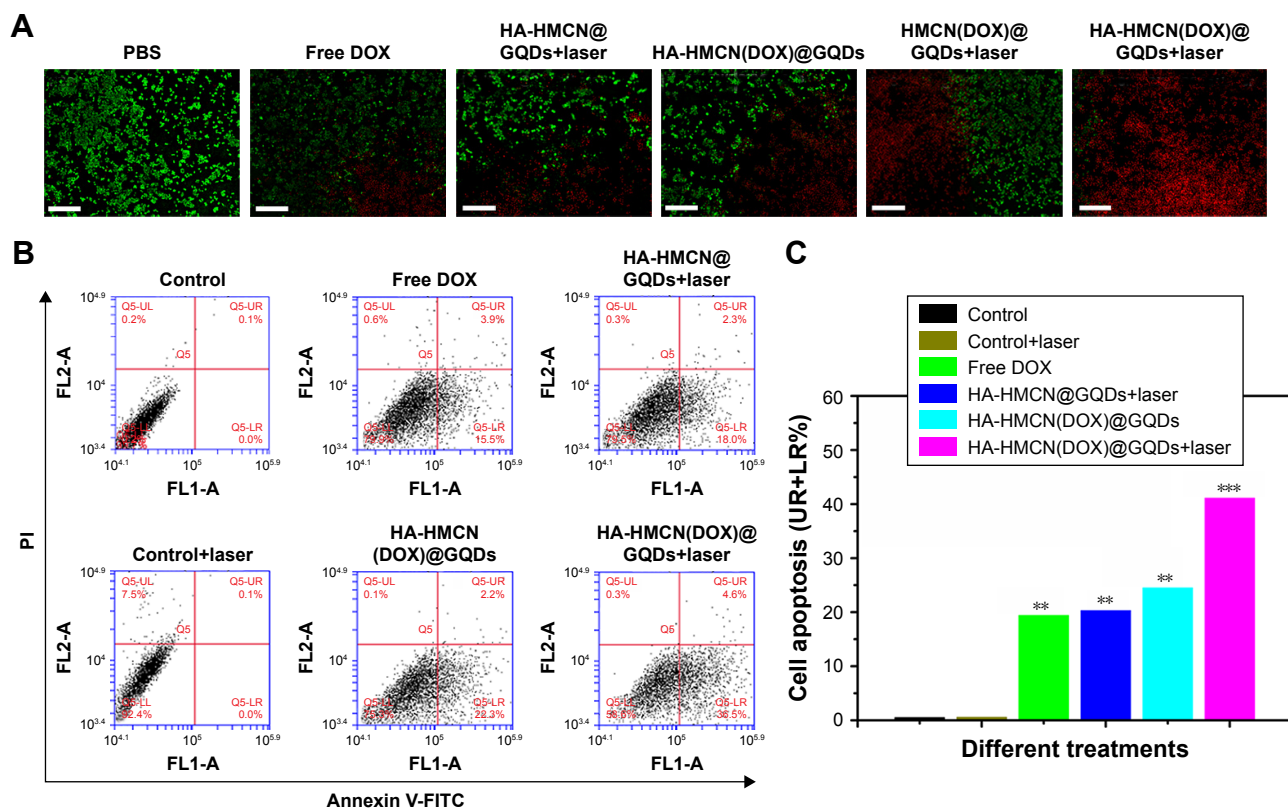


Figure 6 In vitro antitumor activity and cell apoptosis analysis.

Notes: (A) Fluorescence images of HeLa cells co-stained with calcein AM (live cells, green) and PI (dead cells, red) after different treatments: control, free DOX, HA-HMCN(DOX)@GQDs, HA-HMCN@GQDs+laser, HMCN(DOX)@GQDs+laser, and HA-HMCN(DOX)@GQDs+laser. Scale bars: 100 μ m. (B) Flow cytometric analysis of HeLa cells' apoptosis for 12 hours induced by different treatments, performed using Annexin V-FITC/PI staining and (C) the corresponding cell apoptosis analysis. ** and *** respectively indicate $P < 0.01$ and $P < 0.001$ vs control.

Abbreviations: DOX, doxorubicin; FITC, fluorescein isothiocyanate; GQDs, graphene quantum dots; HA, hyaluronic acid; HMCN, hollow mesoporous carbon nanoparticle; PI, propidium iodide.

was about 25%), while the cells treated with PBS and PBS plus NIR exhibited no appreciable apoptosis, demonstrating the biosafety of NIR laser. Meanwhile, the cells treated with HA-HMCN@GQDs with NIR irradiation induced apoptosis up to 20.3%, implying the synergistic photothermal effect of HMCN and GQDs. More importantly, cells treated with HA-HMCN(DOX)@GQDs subjected to NIR irradiation for 5 minutes showed remarkably increased apoptosis rate (41.1%), further confirming the excellent chemo-photothermal capacity of HA-HMCN(DOX)@GQDs for inhibition of tumor cells. It should be noted that there were lesser cells in apoptosis/necrotic status by the treatment of HMCN(DOX)@GQDs under laser irradiation (Figure S5), which may be attributed to the lack of HA modification for targeted cellular uptake enhancement. These results indicated excellent synergistic effect of the HA-HMCN(DOX)@GQDs.

In vivo antitumor efficacy

Encouraged by the attractive therapeutic effect in vitro, we tried to investigate the therapeutic effects of this system in vivo. HeLa tumor-bearing nude mice were used to evaluate

the antitumor efficacy. The mice were i.v. injected with different formulations at a dose of 5 mg/kg of DOX when the tumor volume reached about 100 mm³. For PTT treatment, the mice were irradiated by the 808 nm NIR at a power density of 1 W/cm² for 10 minutes. As illustrated in Figure 7A, the relative tumor volume in the PBS and PBS+NIR groups increased rapidly, and the free DOX (5 mg/kg) could only partially delay the tumor growth due to the shorter half-time and the lower accumulation of free DOX in the tumor site (Figure S6). By contrast, the tumor growth in the HA-HMCN(DOX)@GQDs- and HA-HMCN@GQDs-treated mice with laser irradiation was inhibited to some extent, as the monotherapy (chemotherapy or PTT) was insufficient for effective tumor ablation. As expected, the tumor growth in mice was significantly inhibited after treatment with HA-HMCN(DOX)@GQDs plus 808 nm laser irradiation, which was much better than in any other treatment group. Similarly, the representative photographs (Figure 7B) and the average weight of the tumors (Figure 7C) after 21 days of treatment also demonstrated better therapeutic effect of HA-HMCN(DOX)@GQDs under NIR irradiation. Meanwhile, the body weight

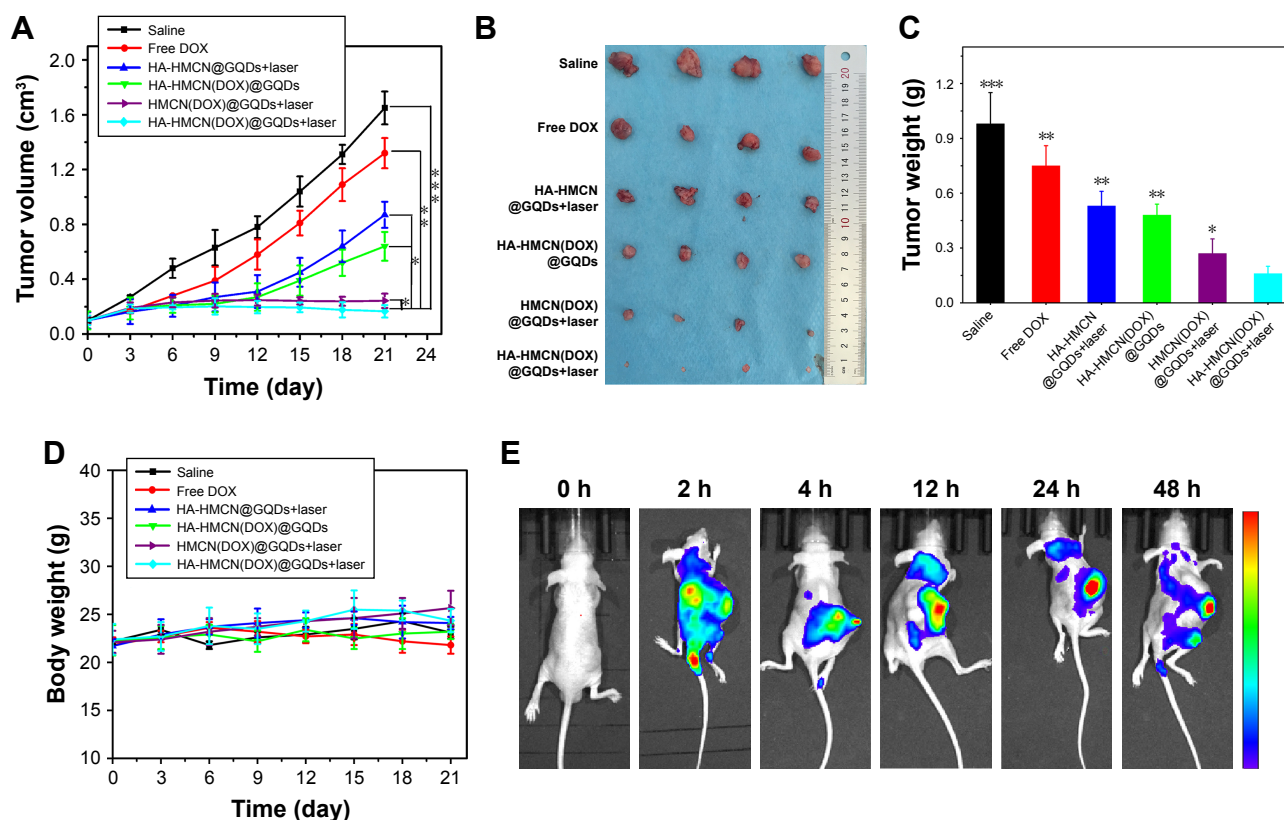


Figure 7 In vivo antitumor activity (n=4).

Notes: (A) Relative tumor volume after different treatments. (B) Representative photographs of the tumors collected from various groups of mice at the end of the treatment (day 21). (C) The tumor weights at the end of therapy on day 21. (D) The body weight of mice during treatment. * $P < 0.05$, ** $P < 0.01$, and *** $P < 0.001$. (E) In vivo fluorescence images of HeLa tumor-bearing nude mice treated with HA-HMCN(DOX)@GQDs under laser irradiation at different time points.

Abbreviations: DOX, doxorubicin; GQDs, graphene quantum dots; HA, hyaluronic acid; HMCN, hollow mesoporous carbon nanoparticle.

of mice was simultaneously measured and no meaningful body weight loss was observed during treatment, indicating no distinct toxic effects of HA-HMCN(DOX)@GQDs (Figure 7D). Collectively, these results confirmed that our HA-HMCN(DOX)@GQDs nanoplateform have great potential as an ideal therapeutic platform for tumor therapy.

Then, in vivo fluorescence imaging was performed after i.v. injection of HA-HMCN(DOX)@GQDs into mice bearing HeLa tumor followed by irradiation with 808 nm NIR at a power density of 1 W/cm² for 10 minutes. Strong DOX fluorescence gradually showed up at the tumor site, suggesting the time-dependent increase in the tumor uptake of HA-HMCN(DOX)@GQDs, and the DOX release was triggered by acid microenvironment and NIR laser irradiation (Figure 7E). Twenty-four hours after the i.v. injection of these nanoparticles, the tumors still displayed strong DOX fluorescence. Thus, these results further illustrated the high tumor uptake of as-prepared HA-HMCN(DOX)@GQDs and also the release of DOX in a slow velocity mode.

Histological analysis

Histology analysis including H&E staining and TUNEL staining was further performed on the tumors after differ-

ent treatments to confirm the in vivo antitumor activity. As expected, the tumor tissues in HA-HMCN(DOX)@GQDs plus NIR-treated group showed absence of minor nuclei as compared to the other three groups (Figure 8A). Similarly, the highest level of TUNEL-positive signals, which represented apoptosis-positive cells, was observed (Figure 8B). These tendencies further demonstrated the efficient synergistic therapy of PTT/chemotherapy, which was consistent with the results of therapeutic assays in vivo. Simultaneously, H&E staining of the main organs (heart, liver, spleen, lung, and kidney) was again performed to evaluate the biosafety. After different treatments, no obvious tissue damage or inflammatory lesion was observed in all major organs (Figure 8A), suggesting the good biocompatibility and biosafety of HA-HMCN(DOX)@GQDs.

In vivo pharmacokinetic assay

For fabricating an ideal drug delivery system, improved circulation is important for increasing the accumulation of the drug. Hence, in vivo pharmacokinetic assay of those nanoparticles was carefully carried out by measuring DOX fluorescence in blood samples at various time points after i.v. injection of different formulations. As shown in Figure S6,

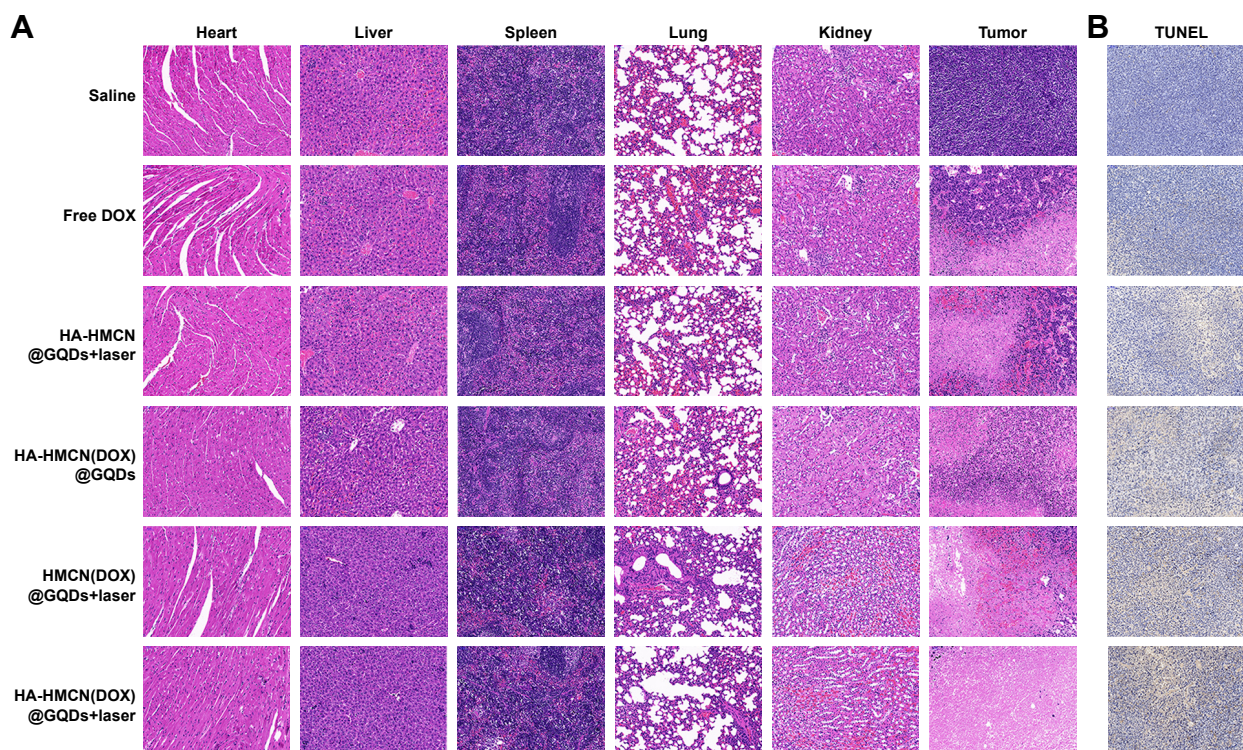


Figure 8 In vivo histological staining.

Notes: (A) H&E staining of the major organs (heart, liver, spleen, lung, and kidney) and tumor tissues collected from different groups after treatment. (B) TUNEL staining on tumor sections after various treatments.

Abbreviations: DOX, doxorubicin; GQDs, graphene quantum dots; HA, hyaluronic acid; HMCN, hollow mesoporous carbon nanoparticle.

both HA-HMCN(DOX)@GQDs and HMCN(DOX)@GQDs showed significant enhancement of blood circulation with long blood half-lives (HA-HMCN(DOX)@GQDs $t_{1/2}=6.12\pm0.45$ hours, HA-HMCN(DOX)@GQDs $t_{1/2}=6.76\pm0.57$ hours), which were much longer than that of free DOX ($t_{1/2}=0.83\pm0.19$ hours). It should be noted that HA-HMCN(DOX)@GQDs and HMCN(DOX)@GQDs exhibited similar blood circulation half-lives, indicating that the HA modification had negligible effect on the pharmacokinetics of HMCN(DOX)@GQDs nanoparticles. Meanwhile, the relative pharmacokinetic parameters of the maximum plasma concentration (C_{max}), area under the plasma concentration vs time curves ($AUC_{0-\infty}$), and the mean residence time of DOX in different formulations are presented in Table S1. These results suggested that the HA-HMCN(DOX)@GQDs nanoparticles could effectively enhance the accumulation and retention of drugs in the tumor tissues to achieve chemotherapeutic efficacy.

Conclusion

To summarize, a multifunctional pH-/NIR-responsive nanoparticle based on HMCN and GQDs was successfully designed for effective chemo-PTT combination therapy and the specific delivery of DOX to CD44 receptor-overexpressing cancer cells. The HA-HMCN(DOX)@

GQDs nanoparticles with a uniform size of 120 nm could efficiently generate heat under NIR irradiation for enhancement of synergistic photothermal efficiency due to the cooperation of HMCN and GQDs. The anticancer drug DOX was used as a model drug, the HA-HMCN(DOX)@GQDs nanoparticles exhibited pH/NIR-controlled drug release behavior, and the NIR laser irradiation also could enhance the cellular uptake. In vivo experimental results suggested that the targeted synergistic chemo-photothermal effect of the HA-HMCN(DOX)@GQDs against HeLa cells was realized. Also, the in vivo experiment demonstrated improved antitumor suppression of HA-HMCN(DOX)@GQDs under NIR irradiation. Meanwhile, no observable toxicity or side effects were found either in vitro or in vivo. Overall, the fabricated nanoparticle may, indeed, be a promising nanoplatform as a biocompatible and multifunctional agent for targeting drug delivery and synergistic chemo-PTT.

Acknowledgment

This work was financially supported by the Huimin project of science and technology in Yunnan Province (2016RA012).

Disclosure

The authors report no conflicts of interest in this work.

References

1. Miller KD, Siegel RL, Lin CC, et al. Cancer treatment and survivorship statistics, 2016. *CA Cancer J Clin.* 2016;66(4):271–289.
2. Dos Santos Ramos MA, Da Silva PB, Spósito L, et al. Nanotechnology-based drug delivery systems for control of microbial biofilms: a review. *Int J Nanomedicine.* 2018;13:1179–1213.
3. Xin M, Ji X, de La Cruz LK, Thareja S, Wang B. Strategies to target the Hedgehog signaling pathway for cancer therapy. *Med Res Rev.* 2018;38(3):870–913.
4. Fan W, Yung B, Huang P, Chen X. Nanotechnology for multimodal synergistic cancer therapy. *Chem Rev.* 2017;117(22):13566–13638.
5. Kim J, Kim J, Jeong C, Kim WJ. Synergistic nanomedicine by combined gene and photothermal therapy. *Adv Drug Deliv Rev.* 2016;98:99–112.
6. Lu N, Fan W, Yi X, et al. Biodegradable hollow mesoporous organosilica nanotheranostics for mild hyperthermia-induced bubble-enhanced oxygen-sensitized radiotherapy. *ACS Nano.* 2018;12(2):1580–1591.
7. Chen W, Ouyang J, Liu H, et al. Black phosphorus nanosheet-based drug delivery system for synergistic photodynamic/photothermal/chemotherapy of cancer. *Adv Mater.* 2017;29(5):1603864.
8. Wang L, Shi J, Zhang H, et al. Synergistic anticancer effect of RNAi and photothermal therapy mediated by functionalized single-walled carbon nanotubes. *Biomaterials.* 2013;34(1):262–274.
9. Li X, Yan Y, Lin Y, et al. Hollow mesoporous carbon as a near-infrared absorbing carrier compared with mesoporous carbon nanoparticles for chemo-photothermal therapy. *J Colloid Interface Sci.* 2017;494:159–169.
10. Lu N, Huang P, Fan W, et al. Tri-stimuli-responsive biodegradable theranostics for mild hyperthermia enhanced chemotherapy. *Biomaterials.* 2017;126:39–48.
11. Yang Y, Aw J, Xing B. Nanostructures for NIR light-controlled therapies. *Nanoscale.* 2017;9(11):3698–3718.
12. Son KH, Hong JH, Lee JW. Carbon nanotubes as cancer therapeutic carriers and mediators. *Int J Nanomedicine.* 2016;11:5163–5185.
13. Liu J, Wang C, Wang X, et al. Mesoporous silica coated single-walled carbon nanotubes as a multifunctional light-responsive platform for cancer combination therapy. *Adv Funct Mater.* 2015;25(3):384–392.
14. Li Z, Hu Y, Howard KA, et al. Multifunctional bismuth selenide nanocomposites for antitumor thermo-chemotherapy and imaging. *ACS Nano.* 2016;10(1):984–997.
15. Wu J, Bremner DH, Niu S, et al. Functionalized MoS₂ nanosheet-capped periodic mesoporous organosilicas as a multifunctional platform for synergistic targeted chemo-photothermal therapy. *Chem Eng J.* 2018;342:90–102.
16. Baeza A, Manzano M, Colilla M, Vallet-Regí M. Recent advances in mesoporous silica nanoparticles for antitumor therapy: our contribution. *Biomater Sci.* 2016;4(5):803–813.
17. Zhang Y, Ang CY, Li M, Tan SY, Qu Q, Zhao Y. Polymeric prodrug grafted hollow mesoporous silica nanoparticles encapsulating near-infrared absorbing dye for potent combined photothermal–chemotherapy. *ACS Appl Mater Interfaces.* 2016;8(11):6869–6879.
18. Liu T, Wang C, Gu X, et al. Drug delivery with PEGylated MoS₂ nano-sheets for combined photothermal and chemotherapy of cancer. *Adv Mater.* 2014;26(21):3433–3440.
19. Chen YW, Su YL, Hu SH, Chen SY. Functionalized graphene nanocomposites for enhancing photothermal therapy in tumor treatment. *Adv Drug Deliv Rev.* 2016;105(Pt B):190–204.
20. Benzigar MR, Talapaneni SN, Joseph S, et al. Recent advances in functionalized micro and mesoporous carbon materials: synthesis and applications. *Chem Soc Rev.* 2018;47(8):2680–2721.
21. Lim WG, Mun Y, Cho A, et al. Synergistic effect of molecular-type electrocatalysts with ultrahigh pore volume carbon microspheres for lithium-sulfur batteries. *ACS Nano.* 2018;12(6):6013–6022.
22. Zhang R, Jiang J, Zhou J, et al. Biofunctionalized “Kiwifruit-Assembly” of oxidoreductases in mesoporous ZnO/carbon nanoparticles for efficient asymmetric catalysis. *Adv Mater.* 2018;30(11):1705443.
23. Zhou L, Jing Y, Liu Y, et al. Mesoporous carbon nanospheres as a multifunctional carrier for cancer theranostics. *Theranostics.* 2018;8(3):663–675.
24. Wu F, Pu N, Ye G, et al. Performance and mechanism of uranium adsorption from seawater to poly(dopamine)-inspired sorbents. *Environ Sci Technol.* 2017;51(8):4606–4614.
25. Huang X, Wu S, du X. Gated mesoporous carbon nanoparticles as drug delivery system for stimuli-responsive controlled release. *Carbon.* 2016;101:135–142.
26. Guiju Xu SL, Niu H, Lv W, Wu Ren’an. Functionalized mesoporous carbon nanoparticles for targeted chemo-photothermal therapy of cancer cells under near-infrared irradiation. *RSC Adv.* 2014;4(64):33986–33997.
27. Zhou L, Dong K, Chen Z, Ren J, Qu X. Near-infrared absorbing mesoporous carbon nanoparticle as an intelligent drug carrier for dual-triggered synergistic cancer therapy. *Carbon N Y.* 2015;82:479–488.
28. Chen Y, Meng Q, Wu M, et al. Hollow mesoporous organosilica nanoparticles: a generic intelligent framework-hybridization approach for biomedicine. *J Am Chem Soc.* 2014;136(46):16326–16334.
29. Zhang Y, Ang CY, Li M, et al. Polymer-coated hollow mesoporous silica nanoparticles for triple-responsive drug delivery. *ACS Appl Mater Interfaces.* 2015;7(32):18179–18187.
30. Ma M, Huang Y, Chen H, et al. Bi₂S₃-embedded mesoporous silica nanoparticles for efficient drug delivery and interstitial radiotherapy sensitization. *Biomaterials.* 2015;37:447–455.
31. Zhao W, Li A, Chen C, et al. Transferrin-decorated, MoS₂-capped hollow mesoporous silica nanospheres as a self-guided chemo-photothermal nanopatform for controlled drug release and chemotherapy. *J Mater Chem B.* 2017;5(35):7403–7414.
32. Lu N, Tian Y, Tian W, et al. Smart cancer cell targeting imaging and drug delivery system by systematically engineering periodic mesoporous organosilica nanoparticles. *ACS Appl Mater Interfaces.* 2016;8(5):2985–2993.
33. Zhang J, Yuan ZF, Wang Y, et al. Multifunctional envelope-type mesoporous silica nanoparticles for tumor-triggered targeting drug delivery. *J Am Chem Soc.* 2013;135(13):5068–5073.
34. Xu Y, Wang X, Zhang WL, Lv F, Guo S. Recent progress in two-dimensional inorganic quantum dots. *Chem Soc Rev.* 2018;47(2):586–625.
35. Qiu J, Zhang R, Li J, et al. Fluorescent graphene quantum dots as traceable, pH-sensitive drug delivery systems. *Int J Nanomedicine.* 2015;10:6709–6724.
36. Zhang J, Yu S-H. Carbon dots: large-scale synthesis, sensing and bioimaging. *Mater Today.* 2016;19(7):382–393.
37. Yao X, Niu X, Ma K, et al. Graphene quantum dots-capped magnetic mesoporous silica nanoparticles as a multifunctional platform for controlled drug delivery, magnetic hyperthermia, and photothermal therapy. *Small.* 2017;13(2):1602225.
38. Chen Y, Chen H, Guo L, et al. Hollow/rattle-type mesoporous nanostructures by a structural difference-based selective etching strategy. *ACS Nano.* 2010;4(1):529–539.
39. Zhao Q, Wang X, Yan Y, et al. The advantage of hollow mesoporous carbon as a near-infrared absorbing drug carrier in chemo-photothermal therapy compared with IR-820. *Eur J Pharm Sci.* 2017;99:66–74.
40. Wang Y, Wang K, Zhao J, et al. Multifunctional mesoporous silica-coated graphene nanosheet used for chemo-photothermal synergistic targeted therapy of glioma. *J Am Chem Soc.* 2013;135(12):4799–4804.
41. Li J, Hu Y, Yang J, et al. Hyaluronic acid-modified Fe₃O₄@Au core/shell nanostars for multimodal imaging and photothermal therapy of tumors. *Biomaterials.* 2015;38:10–21.
42. Chen Y, Li H, Deng Y, Sun H, Ke X, Ci T. Near-infrared light triggered drug delivery system for higher efficacy of combined chemo-photothermal treatment. *Acta Biomater.* 2017;51(15):374–392.
43. Tang Y, Lei T, Manchanda R, et al. Simultaneous delivery of chemotherapeutic and thermal-optical agents to cancer cells by a polymeric (PLGA) nanocarrier: an in vitro study. *Pharm Res.* 2010;27(10):2242–2253.

Supplementary materials

Table S1 Pharmacokinetic parameters of DOX after intravenous injection (n=4)

Parameters	Free DOX	HMCN(DOX)@GQDs	HA-HMCN(DOX)@GQDs
$\tau_{1/2\beta}$ (hours)	0.83±0.19	6.76±0.57	6.12±0.45
C_{max} (µg/mL)	12.84±1.1	16.76±0.72	15.02±1.3
$AUC_{0-\infty}$ (µg/mL·h)	8.67±1.23	104.16±14.35	99.96±12.17
MRT (hours)	0.93±0.26	9.46±1.32	9.15±1.21

Abbreviations: AUC, area under the curve; DOX, doxorubicin; GQDs, graphene quantum dots; HA, hyaluronic acid; HMCN, hollow mesoporous carbon nanoparticle; MRT, mean residence time.

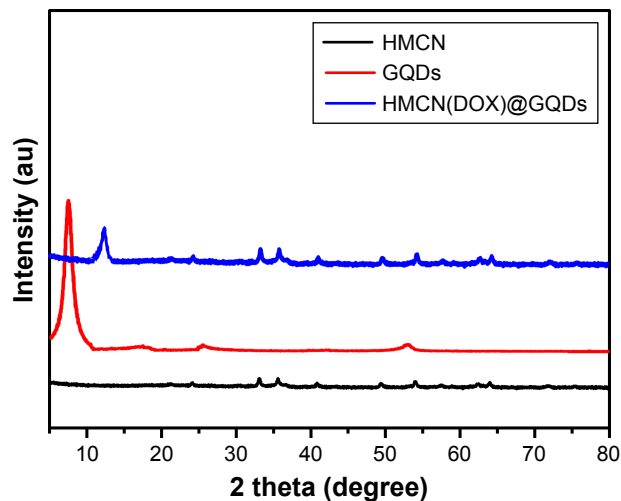


Figure S1 XRD patterns of HMCN, GQDs, and HMCN(DOX)@GQDs.

Abbreviations: DOX, doxorubicin; GQDs, graphene quantum dots; HMCN, hollow mesoporous carbon nanoparticle; XRD, X-ray diffraction.

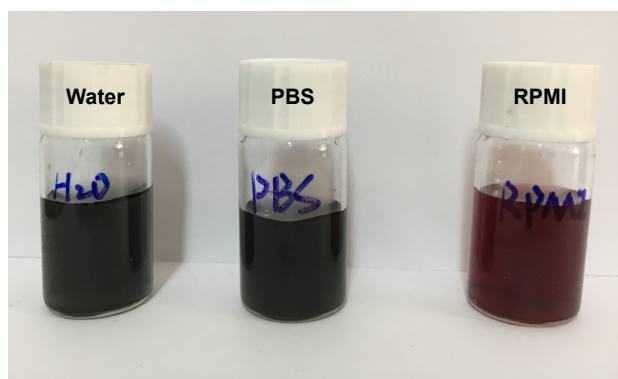


Figure S2 Photograph of HMCN(DOX)@GQDs in water, PBS, and RPMI-1640 medium after allowing to stand for 6 hours.

Abbreviations: DOX, doxorubicin; GQDs, graphene quantum dots; HMCN, hollow mesoporous carbon nanoparticle; RPMI, Roswell Park Memorial Institute.

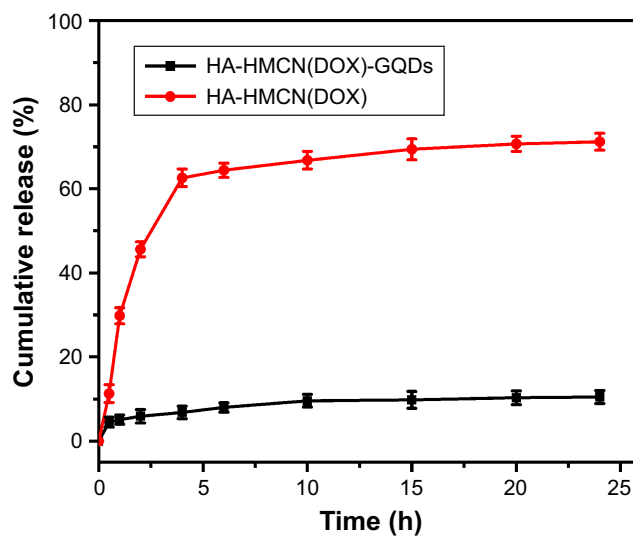


Figure S3 Cumulative DOX release from the HA-HMCN(DOX)@GQDs and HA-HMCN(DOX) nanoparticles at pH 7.4.

Abbreviations: DOX, doxorubicin; GQDs, graphene quantum dots; HA, hyaluronic acid; HMCN, hollow mesoporous carbon nanoparticle.

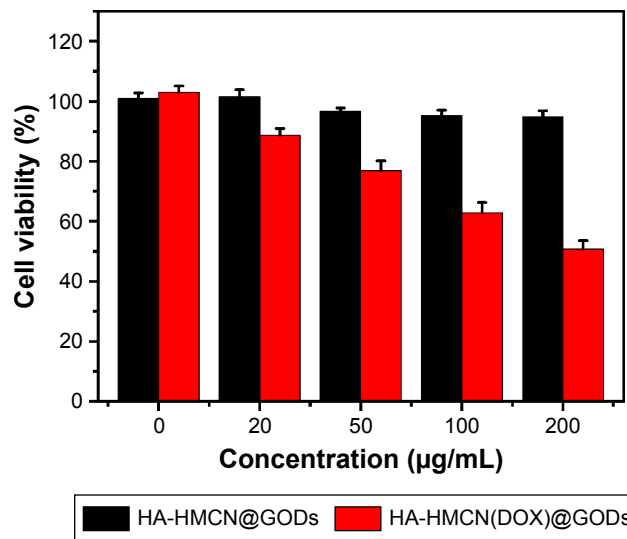


Figure S4 Cell cytotoxicity of HA-HMCN@GQDs and HA-HMCN(DOX)@GQDs against HeLa cells at different concentrations for 24 hours.

Abbreviations: DOX, doxorubicin; GQDs, graphene quantum dots; HA, hyaluronic acid; HMCN, hollow mesoporous carbon nanoparticle.

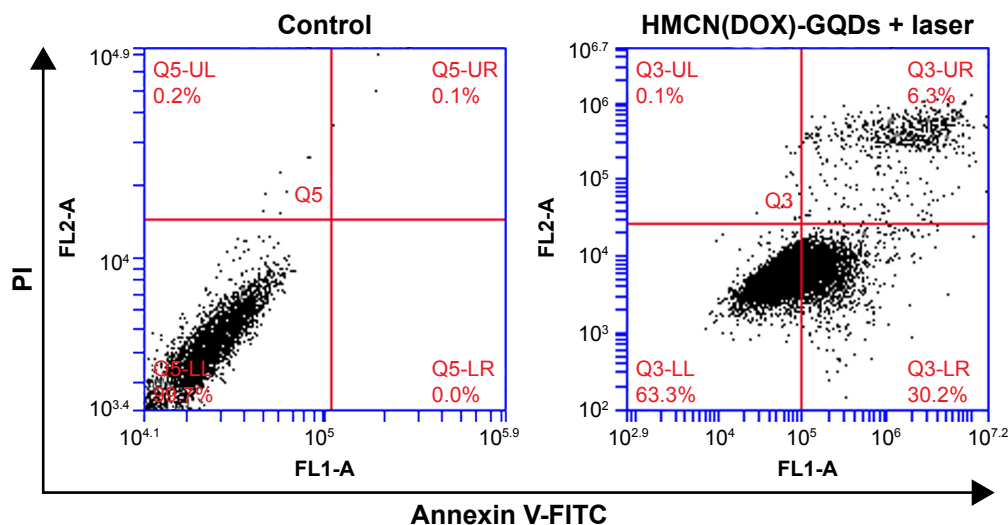


Figure S5 Flow cytometry analysis of apoptosis and necrosis of HeLa cells with blank control and HMCN(DOX)@GQDs under laser irradiation treatment, using the Annexin V-FITC/PI staining.

Abbreviations: DOX, doxorubicin; FITC, fluorescein isothiocyanate; GQDs, graphene quantum dots; HMCN, hollow mesoporous carbon nanoparticle; PI, propidium iodide.

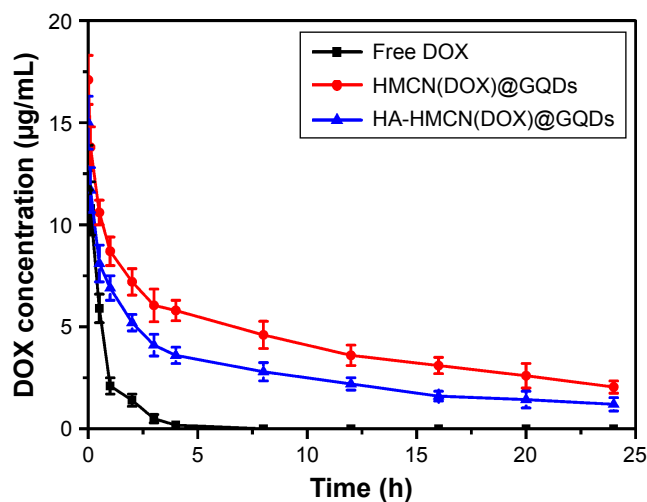


Figure S6 In vivo pharmacokinetics of DOX in blood after free DOX, HMCN(DOX)@GQDs, and HA-HMCN(DOX)@GQDs were intravenously injected into the tumor-bearing mice through the tail vein at a DOX dose of 5 mg/kg (n=4).

Abbreviations: DOX, doxorubicin; GQDs, graphene quantum dots; HA, hyaluronic acid; HMCN, hollow mesoporous carbon nanoparticle.